Dipolar modeling and experimental demonstration of multi-beam plasmonic collimators

New Journal of Physics
The open-access journal for physics

Dipolar modeling and experimental demonstration of multi-beam plasmonic collimators

J-P Tetienne[1], R Blanchard[1], N Yu[1], P Genevet[1,2], M A Kats[1], J A Fan[1], T Edamura[3], S Furuta[3], M Yamanishi[3] and F Capasso[1,4]

[1] School of Engineering and Applied Sciences, Harvard University, Cambridge, MA 02138, USA
[2] Institute for Quantum Studies and Department of Physics, Texas A&M University, College Station, TX 77843, USA
[3] Central Research Laboratory, Hamamatsu Photonics KK, Hamamatsu 434-8601, Japan
E-mail: capasso@seas.harvard.edu

New Journal of Physics **13** (2011) 053057 (8pp)
Received 1 March 2011
Published 27 May 2011
Online at http://www.njp.org/
doi:10.1088/1367-2630/13/5/053057

Abstract. We designed a new class of plasmonic gratings that generate multiple free-space beams in arbitrary directions from a point source of surface waves, using a phenomenological model that accurately predicts their far-field, in amplitude, phase and polarization. We fabricated such gratings on the facets of semiconductor lasers. The plasmonic gratings proposed here are generally relevant to the interfacing of nanoscale optical components to free-space beams. The model introduced here can be used to design general two-dimensional plasmonic gratings.

In recent years, plasmonics, the study of the coupling between electromagnetic fields and electronic oscillations at a metal–dielectric interface, has emerged as one of the most rapidly growing fields of optical physics [1]. Plasmonics has made it possible to move optics to the sub-wavelength scale, opening up a range of new opportunities in science and technology for communication, sensing and imaging [2, 3]. However, for this vision to bear fruit, new components are needed that can act as interconnects between the nanoscale volumes involved in plasmonics and free-space optical elements. Such components would enable the design of complex optical systems where signals, pumps or probes can be sent in and out of photonic waveguides, quantum dots or even single molecules.

[4] Author to whom any correspondence should be addressed.

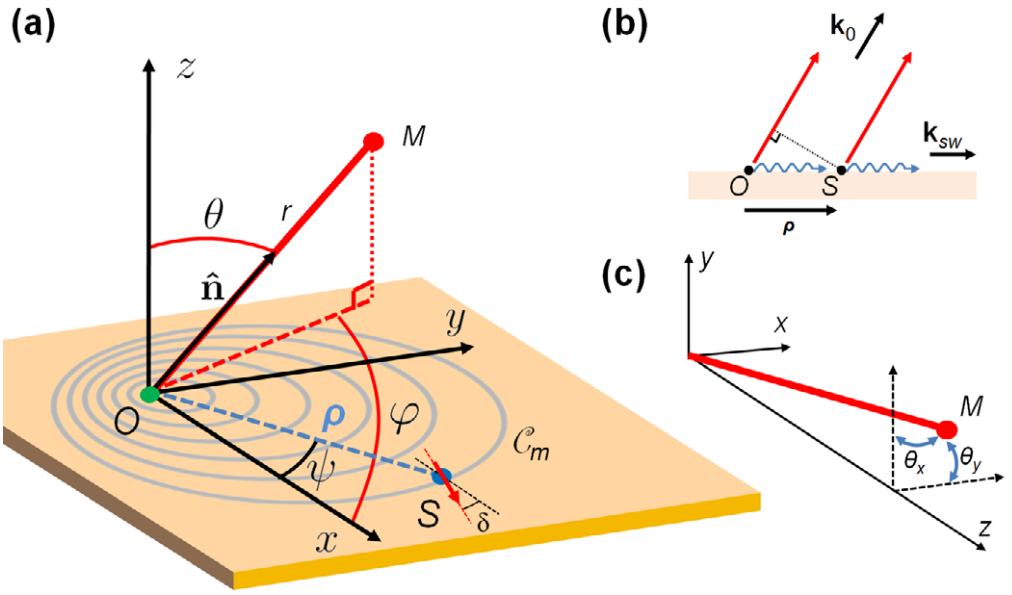

Figure 1. (a) Schematic diagram of a plasmonic lens. (b) Interference between the field radiated by the source O and the field scattered by S. (c) Definition of the angle system (θ_x, θ_y).

The general problem of coupling a surface wave (SW) to free-space beams is usually addressed using one-dimensional (1D) gratings [4–8]. 2D gratings obtained by simple rotation of a second-order 1D grating (also called *bull-eye* structures) were also devised to generate a collimated beam from a point-like source of SWs, or vice versa to focus incident light into a nanoscale-size 'hot spot' ([9–11]; [12] and references therein). Such structures are still 1D in a cylindrical coordinate system. However, designing truly novel 2D structures using standard simulation tools, such as finite-difference time-domain or finite-element methods (FEM), is made very difficult by the large size of the 3D simulations required, typically of the order of 10^7–10^8 mesh cells [13].

The essential physical phenomenon involved in a grating is the interference between the emissions of scatterers distributed along the surface, whether they are holes, particles, grooves or ridges. We introduce here a phenomenological model to calculate the far-field radiation pattern of any 2D grating, which approximates the field scattered by the grating as that of an ensemble of electric dipoles distributed on the surface. The simulation time is reduced to several minutes on a personal computer. While ray tracing models have already been used to describe 2D focusing holographic gratings [14], our dipolar model is more versatile. In particular, by using a 'microscopic' description of the grating, it enables accurate modeling of complex structures with finite size and local parameters that can be varied at will (illumination intensity, scattering efficiency, losses, etc). We use this model to devise a general class of plasmonic lenses that collimate light originating from a single point source and direct it into one or several free-space beams propagating along arbitrary off-axis directions, thus enabling flexible interfacing of plasmonic devices with complex optical systems.

Let us consider a point source O that launches SWs along a corrugated metal–air interface, and an ensemble of point scatterers S lying on the lines $\mathcal{C}_m$ in the x–y-plane (figure 1(a)). A point

source approximates well a source of sub-wavelength dimensions such as an aperture defined in the metallic film. This point source can often be modeled as a point dipole whose polarization imposes a particular angular distribution on the launched SWs [15]. The lines $\mathcal{C}_m$ describe the grooves of a generic 2D grating. We assume that each point S, with polar coordinates (ρ, ψ), scatters a portion of the SWs out of the plane, while the other portion keeps propagating along the surface. The radiation pattern of this system is obtained by summing over all scattered fields.

We assume that the field $\mathrm{d}\mathbf{E}_S(\mathbf{r})$ scattered by an infinitesimal portion of $\mathcal{C}_m$ around S, subtending an angle $\mathrm{d}\psi$, can be modeled by that of an electric dipole located at S, and having an amplitude proportional to the amplitude of the SW at that point, modulated by a scattering efficiency. The SW complex amplitude at S can be expressed as $a_S = f_1(\rho) f_2(\psi) \exp(\mathrm{i}k_{\mathrm{sw}}\rho)$, where $f_1(\rho)$ expresses the decay of the SWs as they propagate away from the source (due to diffraction, scattering and absorption losses), and $f_2(\psi)$ is the angular distribution of the SWs launched at the point source. k_{sw} is the SW wavevector. For a point source polarized at an angle $\psi = \psi_{\mathrm{s}}$, $f_2(\psi)$ can be expressed as $f_2(\psi) = \cos(\psi - \psi_{\mathrm{s}})$ [15]. As the lines of scatterers represent grooves, the orientation of the dipole is taken in the x–y-plane, normal to the groove. Qualitatively, this choice stems from the picture of an incident SW driving charge oscillations on one edge of the groove, which in turn triggers oscillations of image charges on the opposite edge, at the shortest distance and thus in the direction normal to the groove. Polarization-sensitive experimental results will corroborate this assumption (cf figure 3).

If $\hat{\boldsymbol{\delta}}$ is a unit vector that defines the orientation of the dipole, δ being the angle formed with the x-axis, one can write

$$\mathrm{d}\mathbf{E}_S(\mathbf{r}) \propto a_S f_3(\delta - \psi) \frac{\mathrm{e}^{\mathrm{i}(k_0 \hat{\mathbf{n}} \cdot (\mathbf{r} - \boldsymbol{\rho}) + c_1)}}{r} [(\hat{\mathbf{n}} \times \hat{\boldsymbol{\delta}}) \times \hat{\mathbf{n}}] \mathrm{d}\psi, \tag{1}$$

where $\hat{\mathbf{n}}$ is the unit vector in the direction OM. The source is assumed to be monochromatic, with a free-space wavelength $\lambda_0 = 2\pi/k_0$. We neglect the reflections of SWs at the grooves, which is a valid approximation except in the case of constructive interference of the small reflections from each groove, which sets in when the grating period is about $m \cdot \lambda_{\mathrm{sw}}/2$, where $m = 1, 2, 3, \ldots$. The groove scattering efficiency at S is denoted by $f_3(\delta - \psi)$. It depends on the direction of the incident SW relative to the groove, and on the groove depth and width. The phase shift introduced by the scattering event is c_1.

We emphasize that the input parameters of our model (f_1, f_3 and c_1), specific to a given groove geometry and working wavelength, can be readily determined through simple considerations and 2D simulations, as we show thereafter for our particular structure. The simulations we use here require orders of magnitude less resources (in time and memory) than the 3D simulations one would need to perform to simulate the final device. Importantly, once these parameters have been evaluated, it is possible to study the response of all sorts of gratings by simply changing the equation of the curves $\mathcal{C}_m$, predicting not only the amplitude pattern but also the phase pattern of the radiated light.

The expression for the total field is obtained by summing over the continuous distribution of scatterers S on the line $\mathcal{C}_m$, and over N lines. The radiated power density in the far-field is proportional to the angle-dependent component of $|\mathbf{E}(\mathbf{r})|^2$:

$$D(\theta, \varphi) \propto \left| \sum_{m=1}^{N} \int_0^{2\pi} \mathrm{e}^{\mathrm{i}\Delta\phi} f_1 f_2 f_3 \hat{\boldsymbol{e}}(\theta, \varphi, \delta) \mathrm{d}\psi \right|^2, \tag{2}$$

where $\hat{\boldsymbol{e}}(\theta, \varphi, \delta) = \cos(\theta)\cos(\delta - \varphi)\hat{\boldsymbol{\theta}} + \sin(\delta - \varphi)\hat{\boldsymbol{\phi}}$. Here, $\Delta\phi$ is the phase difference between the field $\mathbf{E}_S$ scattered by S and the field $\mathbf{E}_0$ directly emitted from the source O, both evaluated at point M with spherical coordinates (r, θ, φ) in the far-field ($r \gg d \gg \lambda$, the grating dimensions being of order d). It is given by

$$\Delta\phi = k_{\mathrm{sw}}\hat{\mathbf{m}} \cdot \boldsymbol{\rho} - k_0\hat{\mathbf{n}} \cdot \boldsymbol{\rho} + c_1, \tag{3}$$

where $\hat{\mathbf{m}}$ is the unit vector in the direction OS.

The model developed here enables us to calculate the far-field radiation pattern of any 2D grating, once the equation of the curves $\mathcal{C}_m$ is known. We are interested in a particular grating that would scatter SWs originating from a point source into a collimated free-space beam of arbitrary direction (θ, φ). We obtain the equation of the curves $\mathcal{C}_m$ for such a grating by requiring constructive interference in that specific direction. This condition is $\Delta\phi = m2\pi$, with m being an integer. Introducing the SW effective index n_{sw}, we obtain from (3) the equation that yields the position of the scatterers:

$$\rho = \rho_m(\psi) = \lambda_0 \frac{m - c_1/2\pi}{n_{\mathrm{sw}} - \sin(\theta)\cos(\psi - \varphi)}. \tag{4}$$

This equation states that the scatterers must be located on the curves $\mathcal{C}_m$ defined by the polar equations $\rho = \rho_m(\psi)$ for all emitted fields to constructively interfere in the direction (θ, φ). The curves $\mathcal{C}_m$ are ellipses with the origin O at one of their foci. Note that the ellipses $\mathcal{C}'_m$, obtained by translation of the ellipses $\mathcal{C}_m$ in such a way as to position O at the other focus, would lead to constructive interference in the direction $(\theta, \varphi + \pi)$. As our experimental setup scans the far-field in the angle system (θ_x, θ_y), which are the angles with respect to the z-axis projected on the planes x–z and y–z (figure 1(c)), we convert the angle system (θ, φ) into this new one.

From (2) and (4), we are able to calculate the far-field patterns of our elliptical gratings. In order to demonstrate that such elliptical gratings can act as plasmonic lenses, we fabricated the structures directly on the gold-coated facet of mid-infrared quantum cascade lasers (QCLs) emitting at $\lambda = 8.06\,\mu$m, using the process described in [16]. QCLs with small divergence beams are highly desirable. Second-order gratings directly defined on the laser waveguide are often used to obtain surface emission into a beam with reduced divergence in the direction along the laser ridge [17, 18]. Using aperiodic gratings, multi-beam emission has been demonstrated in such structures [19] and collimation in two dimension has been reported for gratings defined on microdisc or ring cavities [20, 21]. However, the solution we present here offers the advantage that it decouples beam engineering from waveguide engineering, providing much more flexibility. Previous demonstrations of multi-beam emission from semiconductor lasers using plasmonic structures defined on their facet relied on simple 1D gratings, which resulted in asymmetric beam shapes [22]. These structures presented limited control over the direction of emission. Here, the application of our dipolar model has enabled us to overcome these limitations by facilitating the design of more complex grating structures. Note also that the concept is general and such lenses can be implemented on any structure supporting SWs or quasi-2D optical modes (e.g. slab waveguides). It is also scalable to other spectral ranges.

We performed 2D simulations of a 1D grating, using a commercial FEM simulation package (COMSOL Multiphysics), in order to design the groove parameters and extract the relevant parameters. Groove depth and width of 1 μm have been found to maximize the peak intensity of the collimated beam for a grating comprising 10–20 grooves. This optimization

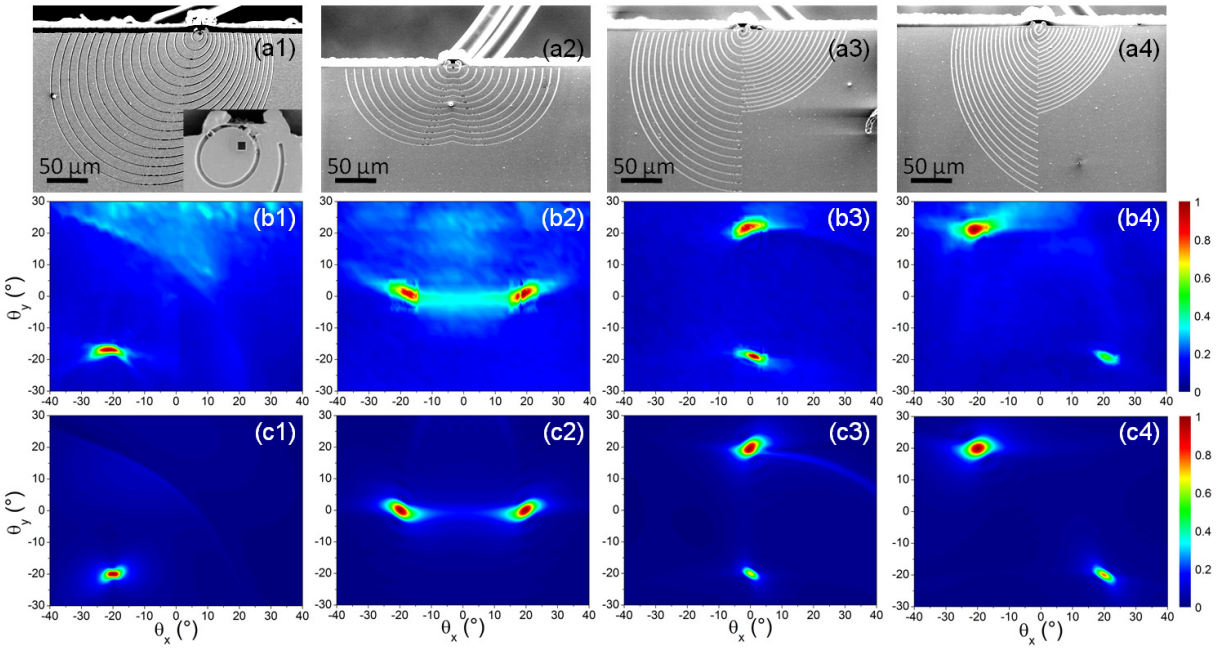

Figure 2. Four different plasmonic lenses producing one (a1) or two (a2, a3, a4) beams, fabricated on the facet of quantum cascade lasers (QCLs). For each structure, we show an SEM image (a), and the measured (b) and calculated (using the model we develop herein) (c) far-field intensities (normalized to 1). The inset of (a1) is a close-up image of a typical aperture. The measured far-fields are obtained by scanning a liquid-nitrogen-cooled mercury–cadmium–telluride detector, positioned 10–20 cm from the device, over θ_x and θ_y, with a resolution of 0.5°.

relies on a trade-off between the grooves' scattering efficiency and the amount of energy reaching the last grooves. With these dimensions, and for an off-resonance grating (i.e. for a grating period different from $m \cdot \lambda_{sw}/2$, where $m = 1, 2, 3, \ldots$), we estimated $n_{sw} \simeq 1.03$ and $c_1/2\pi \simeq 0.23$ at $\lambda = 8.06\,\mu$m. The decay law was found to scale as $\rho^{-1/2}$. This is consistent with the decay of quasi-cylindrical waves (which is the dominant mode of propagation of SWs at long wavelengths [23]) and implies a dependence $f_1(\rho) \propto \rho^{-1}$ for the 3D case. Finally, we neglected the variation of f_3 with ψ since the SWs always impinge on the grooves with an angle close to $\pi/2$ in our small eccentricity elliptical gratings.

Figure 2(a1) shows a scanning electron microscope (SEM) image of a representative fabricated grating, designed to emit light in the direction ($\theta_x = -20°$, $\theta_y = -20°$). In this device, the point-like source of SWs is an aperture opened in the metal film (inset of figure 2(a1)). The light in the laser waveguide impinges on the back of the aperture, launching SWs on the grating–air interface, along with some directly transmitted light. The point-like character of the aperture stems from its subwavelength dimensions ($2\,\mu$m $\times$ $2\,\mu$m for $\lambda = 8.06\,\mu$m).

The fabrication process involves focused ion beam (FIB) milling to sculpt 1 μm wide and 1 μm deep grooves into the semiconductor facet (indium phosphide), then deposition of 250 nm of alumina, acting as an insulation layer, followed by 250 nm of gold. The small aperture in the metal film is eventually opened using FIB [16]. As can be seen in figure 2(a1), only a portion of the grating is fabricated because of the geometry of our laser facet.

Figure 2(b1) presents the measured far-field of the device shown in figure 2(a1), which is composed of 13 grooves described by (4). The direction of highest intensity is centered at ($\theta_x = -21^\circ$, $\theta_y = -17^\circ$). The angular divergence, defined as the full-width at half-maximum (FWHM), is about 8° along θ_x and 3° along θ_y. This divergence angle is comparable to those obtained with simple circular collimator designs [15] and represents a dramatic improvement compared to the divergence angles of about 40° along θ_x and 70° along θ_y for the original unpatterned laser. The small discrepancy between our data and the designed angular direction is due to misalignment of the far-field measurement setup. Note that a residual signal is visible in the upper part of the measured far-field, mainly due to light emitted from the back facet of the laser reaching the detector after undesired reflection on the laser mount. To suppress this signal, high-reflection coatings have been applied to the back facets of the devices subsequently fabricated ((a2), (a3) and (a4)). Moreover, a background, which is measured to be $\sim 10\%$ of the maximum intensity, is present. As only a small portion of the light throughput is coupled into the SWs, the destructive interference between the fields scattered by the grooves and the strong direct emission from the aperture is not complete. This results in the background observed. This coupling efficiency could be greatly increased by patterning the metal around the aperture with subwavelength grooves to reduce the wavevector mismatch between the laser waveguide mode and the SWs, as was demonstrated in the terahertz range by Yu *et al* [13].

These data demonstrate that our 2D plasmonic grating transforms a point source of SWs located at the focal point into a collimated free-space beam in a tailorable direction, i.e. it acts as planar plasmonic lens.

We now show that one can design a plasmonic lens with a single focus capable of forming several beams in arbitrary preselected directions. This is achieved by placing portions of different gratings side by side on the facet. We fabricated three different structures (figures 2(a2–4)), each designed to collimate light in two specific directions, respectively ($\theta_x = \pm 20^\circ$, $\theta_y = 0^\circ$) with $N = 13$ grooves, ($\theta_x = 0^\circ$, $\theta_y = \pm 20^\circ$) with $N = 19$ and ($\theta_x = \pm 20^\circ$ and $\theta_y = \mp 20^\circ$) with $N = 20$. The results are presented in figure 2 (columns 2–4), where both the measured (b) and calculated (c) far-field intensities are plotted. The two collimated beams are clearly distinguishable for each plasmonic lens, proving the robustness of the concept.

Figure 2(c) shows the radiation pattern emitted by the four structures in figure 2(a), calculated using (2) and considering a source polarized along y ($\psi_s = \pi/2$). We included in $\mathbf{E}(\mathbf{r})$ only the fields scattered by the grating. The other contributions due to, for example, the light directly radiated at the aperture will contribute to the background, but will not alter significantly the shape of the collimated beam. Our model aims at elucidating the intrinsic operation of the gratings, and we thus considered them to be free of defects stemming from our specific implementation. For each plasmonic lens, there is good agreement between calculated and measured data (figure 2(b)). The shape of the collimated beams is well reproduced, and the measured divergence angle is generally close to the calculated one (relative error of $\sim 15\%$ on average). The discrepancies are mainly attributed to fabrication defects, in particular the presence on the grating surface of dust particles that open additional scattering channels and reduce the propagation length of the SWs. The finite size of the spot is determined by the SW decay and the size of the grating.

Since our model is vectorial, we can extract the state of polarization of the emitted light. Figure 3 shows the components $|E_x|^2$ and $|E_y|^2$, both calculated and measured (via a polarizer), for the fourth device of figure 2. There is good agreement between experimental and

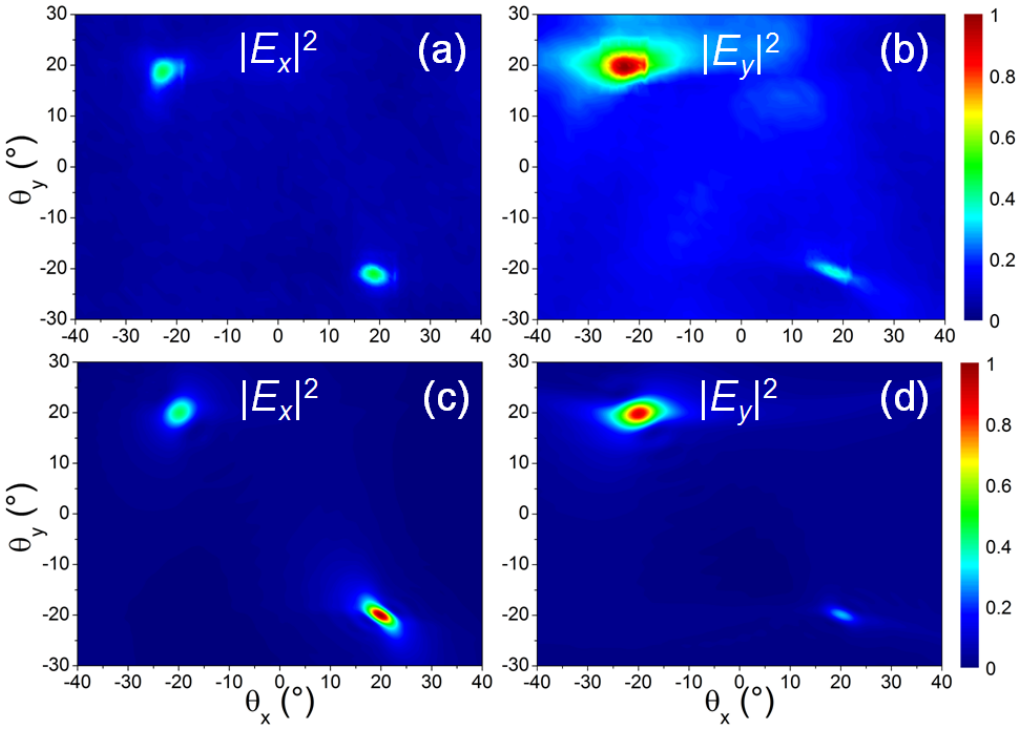

Figure 3. Far-field of the device (4) of figure 2. Measured field intensities $|E_x|^2$ (a) and $|E_y|^2$ (b), normalized to 1. Calculated field intensities $|E_x|^2$ (c) and $|E_y|^2$ (d), normalized to 1.

calculated data, which confirms the validity of our model relying on radiating dipoles oriented perpendicular to the groove tangent.

We finally note that our model also gives the phase profile of the far-field. This model might thus be particularly valuable for designing new plasmonic components featuring complex phase responses, which could generate, for example, Bessel beams or optical vortices.

In summary, we have introduced a phenomenological model for describing 2D metallic gratings. Using this model, we have designed a new class of plasmonic lenses capable of producing multiple free-space beams in arbitrary directions when a point source of SWs is located at their focus. As an example of applications, we have demonstrated dual-beam emission from mid-infrared QCLs and showed the versatility of the concept by realizing different emission directions.

Acknowledgments

We acknowledge support from the Air Force Office of Scientific Research (MURI 67N-1069926) and the Harvard Nanoscale Science and Engineering Center. This work was performed in part at the Center for Nanoscale Systems at Harvard University, a member of the National Nanotechnology Infrastructure Network, which is supported by the National Science Foundation (NSF). JPT is supported by the École Normale Supérieure de Cachan, France. MAK is supported by the NSF through a Graduate Research Fellowship.

References

[1] Maier S A 2007 *Plasmonics: Fundamentals and Applications* (New York: Springer)
[2] Barnes W L *et al* 2003 *Nature* **424** 824
[3] Schuller J A *et al* 2010 *Nat. Mater.* **9** 193
[4] Yu N *et al* 2008 *Nat. Photonics* **2** 564
[5] Martin-Moreno L *et al* 2003 *Phys. Rev. Lett.* **90** 167401
[6] Yu L B *et al* 2005 *Phys. Rev.* B **71** 041405
[7] Garcia-Vidal F J *et al* 2003 *Appl. Phys. Lett.* **83** 4500
[8] Kim S *et al* 2007 *Appl. Phys. Lett.* **90** 051113
[9] Lezec H J *et al* 2002 *Science* **297** 820
[10] Ishi T *et al* 2005 *Japan. J. Appl. Phys.* **44** 364
[11] Liu Z *et al* 2005 *Nano Lett.* **5** 1726
[12] Lee B *et al* 2010 *Prog. Quantum Electron.* **34** 47
[13] Yu N *et al* 2010 *Nat. Mater.* **9** 730
[14] Heitmann D *et al* 1981 *IEEE J. Quantum Electron.* **17** 1257
[15] Yu N *et al* 2010 *IEEE Trans. Nanotechnol.* **9** 11
[16] Yu N *et al* 2008 *Opt. Express* **16** 19447
[17] Hofstetter D *et al* 1999 *Appl. Phys. Lett.* **75** 3769
[18] Schrenk W *et al* 2000 *Appl. Phys. Lett.* **77** 2086
[19] Mahler L *et al* 2010 *Nat. Photonics* **4** 165
[20] Mujagic E *et al* 2008 *Appl. Phys. Lett.* **93** 161101
[21] Mahler L *et al* 2009 *Nat. Photonics* **3** 46
[22] Yu N *et al* 2009 *Appl. Phys. Lett.* **95** 161108
[23] Lalanne P *et al* 2009 *Surf. Sci. Rep.* **64** 453